scientific reports

OPEN

Research on the failure law and actual measurement of floor in extremely close distance thick coal seam mining

Yupei Deng[1,2 ✉], Weidong Pan[1,2], Chao Ma[1,2], Shiqi Liu[1,2], Zhining Zhao[1,2], Cang Deng[1,2] & Meng Li[3]

The vigorous mining of domestic coal resources is accompanied by the complexity and diversification of the conditions of coal seams. Multi seam and close distance coal seam mining have become normalized. For research on the failure law and actual measurement of floor in extremely close distance thick coal seam mining, the paper takes the 30,507 working face of Tashan Coal Mine of China Coal Datong Energy Co., Ltd (Xiaotashan Coal Mine) as the background, obtains the characteristics and scope of the floor failure of the coal seams in the working face through theoretical analysis and numerical calculation, and uses the single hole (Direct Current) DC floor detection technology to carry out on-site measurement. Research has shown that due to the repeated disturbance effects of multilayer coal mining, the lower coal seam floor is prematurely damaged, with a large impact range, and the theoretical characteristics of the overall "lower three zones" of the floor are obvious; The measured maximum damage depth is 16.1 m, and it tends to stabilize within a range of 16 m behind the working face. Single-hole DC detection technology exhibits reliability and accuracy for detecting the damage of coal seam mining floor under complex geological conditions, and this study provides some guidance for the control and detection of rock strata at the bottom of coal seam mining under different geological conditions.

Keywords Extremely close distance coal seams, Floor failure, DC method, Field measurement

The Datong mining area is one of the earliest and largest coal resource development areas in China[1–3]. The mining depth, coal seam occurrence conditions, and difficulty of coal mining are constantly increasing with the development of resources[4]. At the same time, the risks associated with mining are becoming increasingly prominent, among which the risk of groundwater inrush is a major issue[5,6]. Compared to ordinary single coal seam mining, the occurrence conditions of extremely close distance coal seams have repetitive disturbance characteristics, and the rock failure laws are more complex[7]. Bottom water inrush accidents occur during disaster exploration and floor grouting work, which are part of the preparatory work before mining. Through research on practical production problems, it has been found that the probability of floor water inrush accidents occurring during the production process of the working face is higher[8]. The extraction of coal seams can cause instability and damage to the surrounding rock mass, and the repeated disturbances generated by close distance coal seam mining will once again affect the already damaged rock mass. The constantly loose rock mass and changing pore structure increase the permeability of the rock mass and the risk of water inrush[9,10]. Research on the damage law of the working face floor affected by mining is an important part of ensuring safe and efficient production in coal mines.

This is a widely used research method that involves indoor experiments, analytical calculations, and on-site measurements to study floor issues in coal seam mining. Conventional indoor experiments include similarity simulation and numerical simulation, modeling with similar materials or numerical calculations, by establishing a model that approximates actual production, collecting floor stress data, and observing the failure mode of surrounding rock, research is conducted. Analytical calculations include formulas for water inrush coefficient[11,12],

[1]Engineering Research Center for Green and Intelligent Mining of Thick Coal Seam, Ministry of Education, Bejing 100083, China. [2]School of Energy and Mining Engineering, China University of Mining and Technology-Beijing, Beijing, China. [3]Tashan Coal Mine, China Coal Datong Energy Co., Ltd, Datong 037001, Shanxi, China. ✉email: 759239295@qq.com

the "lower three zones" theory[13,14], in-situ tensile and zero position failure theory[15], and multi factor prediction models[16] to estimate the expected depth of floor failure. However, coal seam mining is a massive project with a complex process and multiple factors that affect the stability of the floor. Moreover, mining is carried out dynamically, and the stress and shape of the bottom rock mass are constantly changing. Therefore, the results of the general failure depth obtained solely through indoor testing and theoretical analysis methods often have certain deviations from the on-site measured results[17–22]. Relatively speaking, on-site testing is the most accurate and effective method to verify the depth of mining induced damage to the floor of the working face[23–25].

In recent years, an increasing number of new methods and technologies have been applied to the study of the depth of floor damage in coal mine working faces. Among them, the most widely used and effective is in-situ testing technology, mainly using drilling injection (pressure) method and geophysical methods. Among them, geophysical methods have obvious advantages, such as high efficiency, no damage, low cost, and high accuracy. Wang[26] et al. the electrical characteristics of the working face floor rock during coal mining were measured using the electrical profiling method, and the depth of floor failure was studied through its variation characteristics. Gao[27–29] et al. Yue[30] et al. using direct current method to measure the resistivity characteristics of overlying strata during failure, and judging the rock failure law through spatiotemporal evolution. Daily[31] et al. the electrical method technology of parallel detection using dual lane layout was used to investigate the occurrence of bottom water and the distribution range of thin coal seams. Zhang[32] et al. real time measurement of floor rock resistivity based on high-resolution electrical instrument, and study of floor failure in pressurized underwater mining using similar simulation experiments. High density electrical method was used to detect the depth of floor damage in similar experiments of pressurized coal seam mining. The resistivity CT testing technology has been applied by Liu[33] et al., Zhang[34] et al. and others to detect the process of bottom rock layer damage. Wang[35] et al. measure the range of mining impact on the floor of the working face based on transient electromagnetic method.

A large amount of research by domestic and foreign scholars has verified the reliability of electrical technology in detecting the range of rock mass failure in mines. However, common testing methods have complex systems, long preparation cycles, and multiple collaborative personnel, which make it difficult to use rock mass failure testing on a large scale and cover the entire production process of the working face. By improving the electrical detection equipment and optimizing the testing process, the single hole pre embedded electrode DC method used in this article can effectively reduce the preparation workload in the early stage of actual measurement. At the same time, a single person can complete data acquisition in a single time, and the entire detection process can be flexibly adjusted according to the on-site production arrangement. According to the background of the 30,507 working face of Xiaotashan Coal Mine and the on-site production situation, a test plan for the failure of the working face floor was designed using single hole DC technology. Combining traditional plastic slip line field theory and numerical simulation, the characteristics and maximum depth of the floor failure in extremely close distance coal seam mining were comprehensively studied. It is of great significance to study the control and detection of the bottom rock strata in coal seam mining under different geological conditions.

Overview of the research mining area

The 30,507 working face of Xiaotashan Coal Mine is mining the combined coal seams 3–5, with an average thickness of 17.93 m and a distance of 1.55~6.67 m from the already mined out coal seam 2, with an average of 4.35 m. The direct top thickness of the coal seam is 3–5 m, consisting of high-grade mudstone and carbonaceous mudstone; The basic top thickness of 6–15 m is medium coarse sandstone. The average thickness of the floor is 3.5 m, consisting of sandy mudstone and siltstone. The working face has a length of approximately 1666.94 m, an inclination length of approximately 193 m, and a coal seam inclination angle of 2 °. The ground elevation of the 30,507 working face is +1325~+1480 m, and the coal seam floor elevation is +1000.97~+1018.83 m. The water level elevation is +1013~+1045 m, and the floor trend is high in the south and low in the north. The working face is all under pressure. The location map of 30,507 working face of middling coal Tashan Coal Mine is shown in Fig. 1, and the comprehensive histogram of the working face is shown in Fig. 2.

Theoretical analysis of bottom slip line in extremely close coal seam mining

The slip line theory[2] analyzes the stress on the floor of the working face, causing shear failure and plastic flow along the direction of the failure surface (Fig. 3). Zone I ABE forms a compacted failure zone under the coal wall due to the influence of supporting pressure; The BCE in Zone II undergoes tensile deformation in the horizontal direction due to compression, forming a transition failure zone consisting of a logarithmic spiral and a radial line from point O; The CDE in Zone III is located below the goaf and is a passive failure zone that develops towards the goaf due to the compression of the transition zone.

Maximum plastic failure range of the floor h_0 is:

$$h_0 = \frac{L_0 \cos\phi_0}{2\cos\left(\frac{\pi}{4} + \frac{\phi_0}{2}\right)} e^{\left(\frac{\pi}{4} + \frac{\phi_0}{2}\right)\tan\phi_0} \tag{1}$$

The maximum depth position l_0 is:

$$l_0 = \frac{L_0 \sin\phi_0}{2\cos\left(\frac{\pi}{4} + \frac{\phi_0}{2}\right)} e^{\left(\frac{\pi}{4} + \frac{\phi_0}{2}\right)\tan\phi_0} \tag{2}$$

In the formula, ϕ_0 is average internal friction angle (°), L_0 is wide plastic zone of coal wall(m).
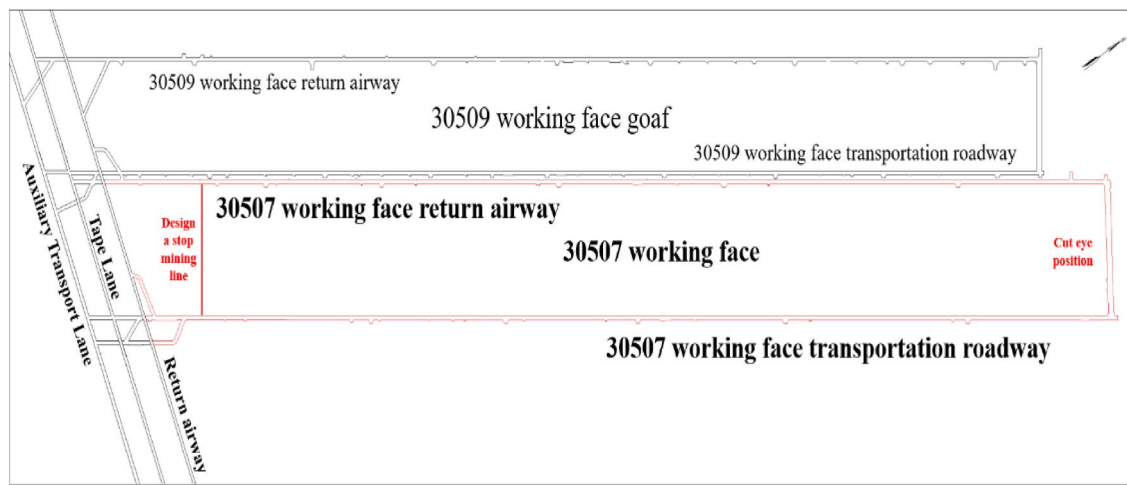
Fig. 1. Location of 30,507 working face.

According to the parameters of the 30,507 working face, $H = 427$ m, $m = 18$ m, and other rock parameters are listed in Table 1. Based on experience, $L_0 = 0.015H$, then $h_0 = 14.37$ m, $l_0 = 11.63$ m. The maximum depth of damage to the floor is 14.37 m, located 11.63 m behind the coal wall.

The law of floor failure in extremely close distance coal seam mining

Based on the geological conditions of the 30,507 working face and the actual production situation, using discrete element numerical simulation analysis software, a calculation model with a length of 400 m and a height of 200 m is established. The upper boundary is modeled at half the burial depth, with fixed support on both sides and the bottom boundary. A vertical compressive stress of $\sigma_{yy} = 7$ MPa is applied to the upper boundary, and leave a 100 m wide coal pillar to eliminate the influence of the boundary. The model layers and joint conditions are shown in Fig. 4. By simulating the mining of No.3–5 coal seams for 200 m under the goaf of No.2 coal seam, with a working face advancement step of 10 m, to study the evolution process and depth of floor damage during close distance coal seam mining. The relevant parameters of the coal seam and rock strata in the model are obtained through laboratory mechanical tests, and the parameters are shown in Table 1.

As the working face advances, the stress changes from the original rock stress state, leading to the formation of plastic failure zones in the coal rock layer. The evolution law of the plastic zone is one of the basis for judging the activity law of the rock layer. It is generally believed that the concentrated area of tensile failure in the rock layer is where the rock layer fractures. By analyzing the evolution law of the plastic zone in the floor area, the activity law is analyzed. In the following model diagram, purple represents tensile failure, red represents critical failure state, and green represents plastic failure.

The mining of No.2 coal seam has a certain impact on the stability of No.3–5 coal seams. When the mining advances to 80 m (Fig. 5), the depth of floor damage reaches its maximum value, and the impact range extends from No.3–5 coal seams to No.6 coal seam. From the development of the plastic zone on the floor, it can be seen that the damage mainly occurs in the older rock layers between No.2 and No.3–5 coal seams. The plastic fracture lines of No.3–5 coal seams gradually decrease from shallow to deep, and there are occasional plastic failures in the sandy mudstone of the floor and No.6 coal seam.

Affected by the mining of the upper No. 2 coal seam, the damage range of the plastic failure zone of the floor in the early stage of the mining of No. 3–5 coal seams has significantly increased. The working face advances 10 m, the plastic zone of the floor develops 9 m and the advance impact range is 30 m (Fig. 6 (a)); When the working face was pushed up to 50 m, it came under pressure for the first time and the floor is significantly compressed. The plastic zone of the floor developed to 13.5 m, the advance impact range is 33.5 m (Fig. 6 (b)); After the working face continued to advance 20 m, the plastic zone of the floor reached its maximum development of 17.7 m, and the leading influence range slightly decreases by 26.5 m (Fig. 6 (c)). At the end of model computation (Fig. 6 (d)), determine through plastic zone, maximum depth stabilizes at 17.7 m and failure line tends towards a "saddle shape".

Actual measurement of maximum damage depth of the floor
Testing techniques and solutions

The actual measurement is based on the single hole DC symmetrical quadrupole electrical profiling technology, and the method of directional drilling and pre-embedded measurement lines is used to accurately locate the measurement points and improve the measurement accuracy. Single hole DC technology has the advantages of short preparation period, simple early construction, short preparation time, and convenient measurement. Pre embedded sealing installation makes the equipment highly adaptable to different geological conditions.

Thickness (m)	Columnar 1: 200	Rock type	Lithology description
43.1		Sandy mudstone / Siltstone / Medium grained sandstone / Coarse grained sandstone	Composed of gray, grayish yellow, purple red sandy mudstone, siltstone, and medium coarse sandstone.
3.71		Medium coarse sandstone	Gray white medium coarse grained quartz feldspar sandstone, with moderate sorting, developing sub angular and wedge-shaped bedding, integrated with the underlying strata.
8.25		Sandy mudstone	Gray and dark gray sandy mudstone, siltstone and light gray, gray white clastic rock, interbedded with thin layers of mudstone and carbonaceous mudstone, containing extremely unstable Shan 2 and Shan 4 coal seams, with locally deposited igneous rocks.
0.34		Mountain 2 Coal	
51.4		Siltstone	
		Mountain 4 Coal	
		Clastic rock	
1.87		Fine and coarse sandstone	Composed of gray fine and coarse-grained sandstone, mainly composed of quartz, locally transformed into sandy mudstone.
14.79			
2.56		Siltstone / Sandy mudstone	Dark gray and gray black siltstone, sandy mudstone, containing plant fossil fragments.
8.28			
3.00		No.2 coal seam	It exists in the entire area, including 1-3 layers of dirt bands.
4.35		Gaoling rock / Gaoling mudstone	Gray and gray brown kaolinite and kaolinite mudstone, with sandy and shell like fractures.
17.93		No.3-5 coal seam	The entire area is developed, with stable coal seams and complex structures, containing 5-10 layers of interbedded gangue. The interbedded gangue consists of kaolinite mudstone and carbonaceous mudstone, which are the main coal seams that can be mined in this area.
3.35			
1.11		Siltstone / Sandy mudstone	The top is composed of high-grade mudstone and sandy mudstone, locally interbedded with unstable coal seam 6. The middle is a set of gray white clastic rocks, interbedded with extremely unstable coal seam 7. The lower part is composed of black colored sandstone and sandy mudstone, containing siderite nodules.
4.63		No.6 coal seam	
1.72		Clastic rock / No.7 coal seam	
20.96		Siltstone / Sandy mudstone	
3.91		No.8 coal seam	Mainly capable of mining stable coal seams, containing 1-2 layers of interbedded gangue.
7.59		Gaoling rock	Gray and gray brown kaolinite, containing sand, locally intercalated with 8 coal seams.
1.80		No.9 coal seam	Gray and gray brown kaolinite, containing sand, locally intercalated with 8 coal seams.
6.48		Gaolingyan / Sandy mudstone / Siltstone	Composed of detrital kaolinite, sandy mudstone, and siltstone.
1.66		Coarse grained sandstone	Gray white medium coarse sandstone, mainly composed of quartz.

Fig. 2. Comprehensive bar chart of 30,507 working face.

The YDZ (A) DC resistivity meter used for testing has a dynamic range of 130db and a measurement sensitivity of 1 microvolt. Measuring points are arranged at equal intervals along the same section of the floor to maintain a certain distribution range of current field. Every four equally spaced measuring points form a detection unit (Fig. 7). The continuous electrodes are taken as the detection range at one time, the electrode interval is taken as the detection range at two times, and the electrode interval is taken as the detection range at three times. The voltage $\triangle U$ and current I per unit time during the detection are recorded at the stationary point, and calculate the apparent resistivity using the formula:

$$K = \pi \cdot AM \cdot AN/MN \tag{4}$$
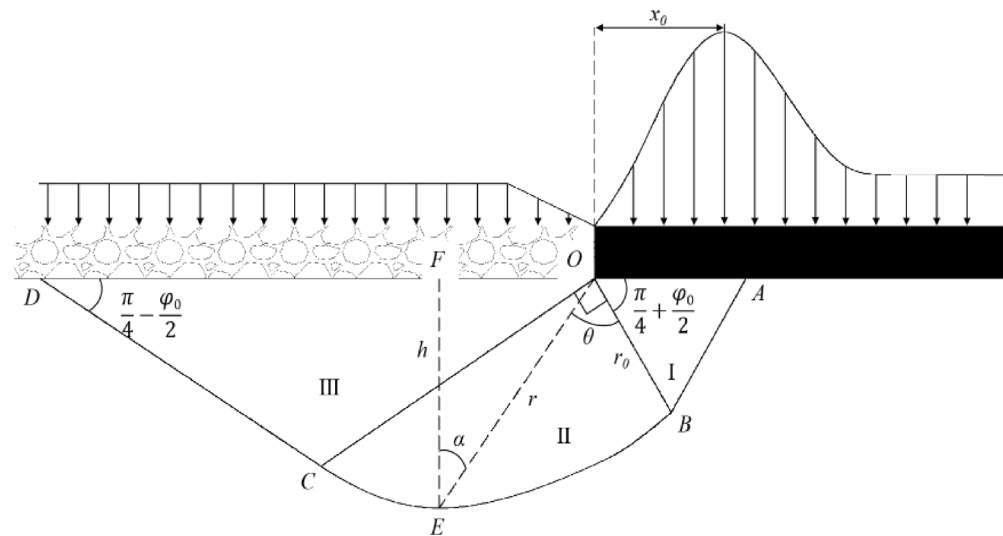
Fig. 3. Maximum depth of floor failure slip line field.

Lithology	Thickness/m	Density/kg·m⁻³	Bulk modulus/GPa	Shear modulus/GPa	Cohesion/MPa	Internal friction angle/°
Sandstone	45	2560	11.1	8.9	3.72	37.57
Medium coarse sandstone	12	2600	11.7	9	6	38
Siltstone	51	2500	10.2	8.4	3.72	36.4
Mountain 4 Coal	1.8	1400	3.48	0.78	1.43	34.5
Clastic rock	15	2600	11.7	9	6	38
Fine Sandstone	2.5	2620	12.2	10	6.2	39
Sandy mudstone	8	2340	9	8	5.5	36
No.2 coal seam	3	1400	3.48	0.78	1.43	34.5
Gaoling rock	4.3	2100	8.2	7.6	5.5	35
No.3–5 coal seam	18	1320	5.4	1.96	1.6	39
Sandy mudstone	3.3	2340	9	8	5.5	36
No.6 coal seam	1.1	1400	3.48	0.78	1.43	34.5
Clastic rock	4.6	2560	11.1	8.9	3.72	37.57
No.7 coal seam	1.7	1400	3.48	0.78	1.43	34.5
Siltstone	21	2500	12.2	8.4	3.72	38

Table 1. Rock physical and mechanical parameters.

The test results located outside the mining influence range in the early stage of the test are taken as the reference value of apparent resistivity (original rock state). The working face is advanced to the testing range, and periodic measurements are taken at each measuring point to obtain the apparent resistivity values of measuring points at different depths during the mining period. Usually, the development of fractures accompanied by rock mass failure can cause fluctuations in apparent resistivity. When the fractures expand and there is no groundwater influence, the apparent resistivity increases, and when the fractures are filled with groundwater, the apparent resistivity will significantly decrease. In the early stage of mining, the bottom rock layer is disturbed and damaged, and the apparent resistivity fluctuates according to the underground rock mass occurrence conditions. In the later stage of mining, the cracks in the floor gradually close due to the compaction effect of the top plate, and the apparent resistivity may fall back and stabilize.

In order to accurately locate the positions of each measuring point and improve the detection accuracy, the test borehole was inclinedly positioned before embedding the lateral line. The final measured observation borehole inclination length was 83 m and the borehole depth was 20.57 m (Fig. 8). The inclinometer positioning data is shown in Table 2.

The observation hole opening is equipped with a 4 m long protective casing, and 37 power supply electrodes are arranged at equal intervals from the bottom of the casing to the bottom of the drilling hole, forming 34 sets of measurement points. The observation line is 74 m long, and the maximum vertical depth of observation is 18.8 m.

Determine the actual measurement plan based on the production progress of the 30,507 working face and the layout of the testing cables. The testing will be conducted in three stages: the first stage will measure every
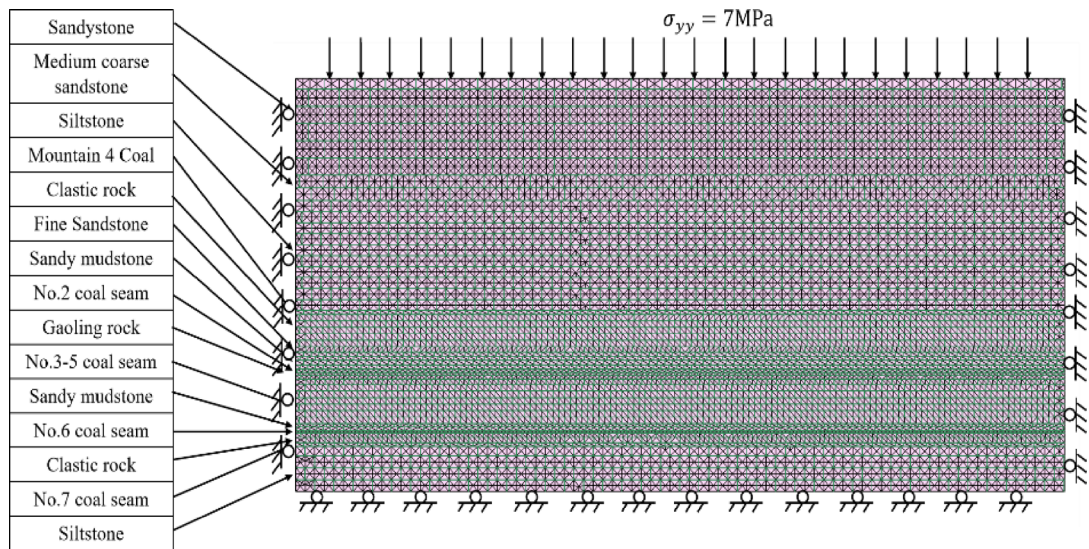
**Fig. 4.** Numerical simulation model and interlayer structure of coal seams.
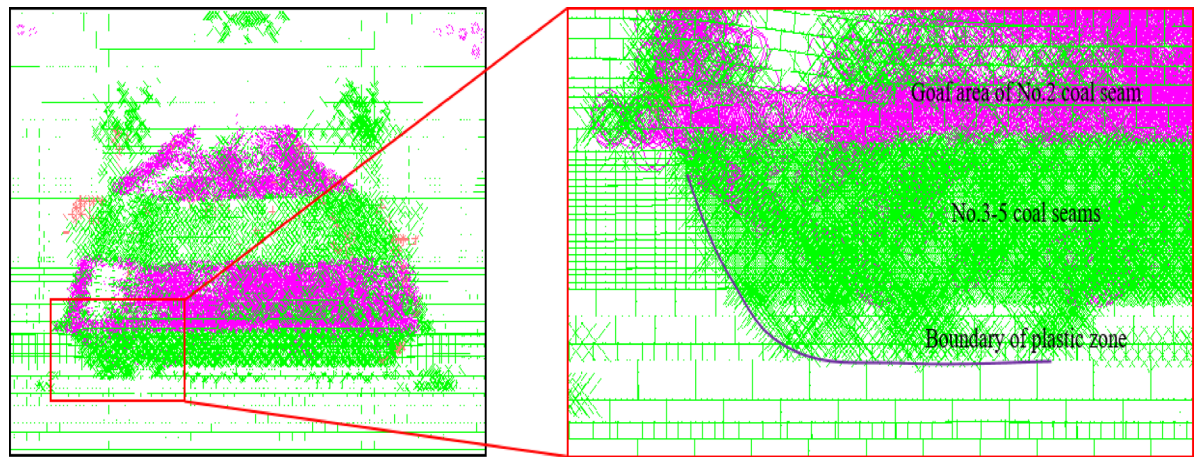
Fig. 5. The range of plastic zone on the floor after the extraction of No. 2 coal seam.

four days, the second stage will measure every two days, and the third stage will measure every day, ensure that the measured data density meets the analysis requirements. The test lasted for 18 days and obtained 9 sets of resistance data for the substrate. Relationship between detection process and working face position is shown in Fig. 9. Analyze the distribution pattern of resistivity using the geometric relationship between each electrode and the substrate, and measure the electrode distance and power supply electrode distance using single distance, double distance, and triple distance methods.

Analysis of actual test results

From the single distance difference plot (Fig. 10), divided by measuring point 28, the upper measuring points have varying degrees of changes due to mining effects, while the lower measuring points have little fluctuation compared to the initial values. The measurement points affected by mining showed a sudden change in initial values, followed by a reverse change, and finally a gradually stable trend of change. After the 28th measuring point, the difference between each measuring point and the background value is basically the same, indicating that the corresponding layer of the deep measuring point after the 28th measuring point has not been damaged by mining, so the maximum damage location is the depth corresponding to the 28th measuring point.

Compared with the observation curve of the same single distance, due to the increase in polar distance, the detection distance of double distance and triple distance is farther, and the apparent resistivity data is larger. The fluctuation of the double distance detection pattern occurs farthest at measurement point 27 (Fig. 11), and the fluctuation of the triple distance detection pattern occurs farthest at measurement point 27 (Fig. 12).

By observing the numerical changes at different stages of each measuring point (Fig. 13), it can be seen that each measuring point shows a development trend of first increasing, then decreasing, and finally oscillating and stabilizing, which is consistent with the change process of the coal seam floor being first compacted by supporting

(a) The plastic zone range of the 10m floor of coal No. 3-5 is pushed forward

(b) The plastic zone range of the 50m floor of coal No. 3-5 is pushed forward

(c) The plastic zone range of the 70m floor of coal No. 3-5 is pushed forward

(d) The plastic zone range of the 200m floor of coal No. 3-5 is pushed forward
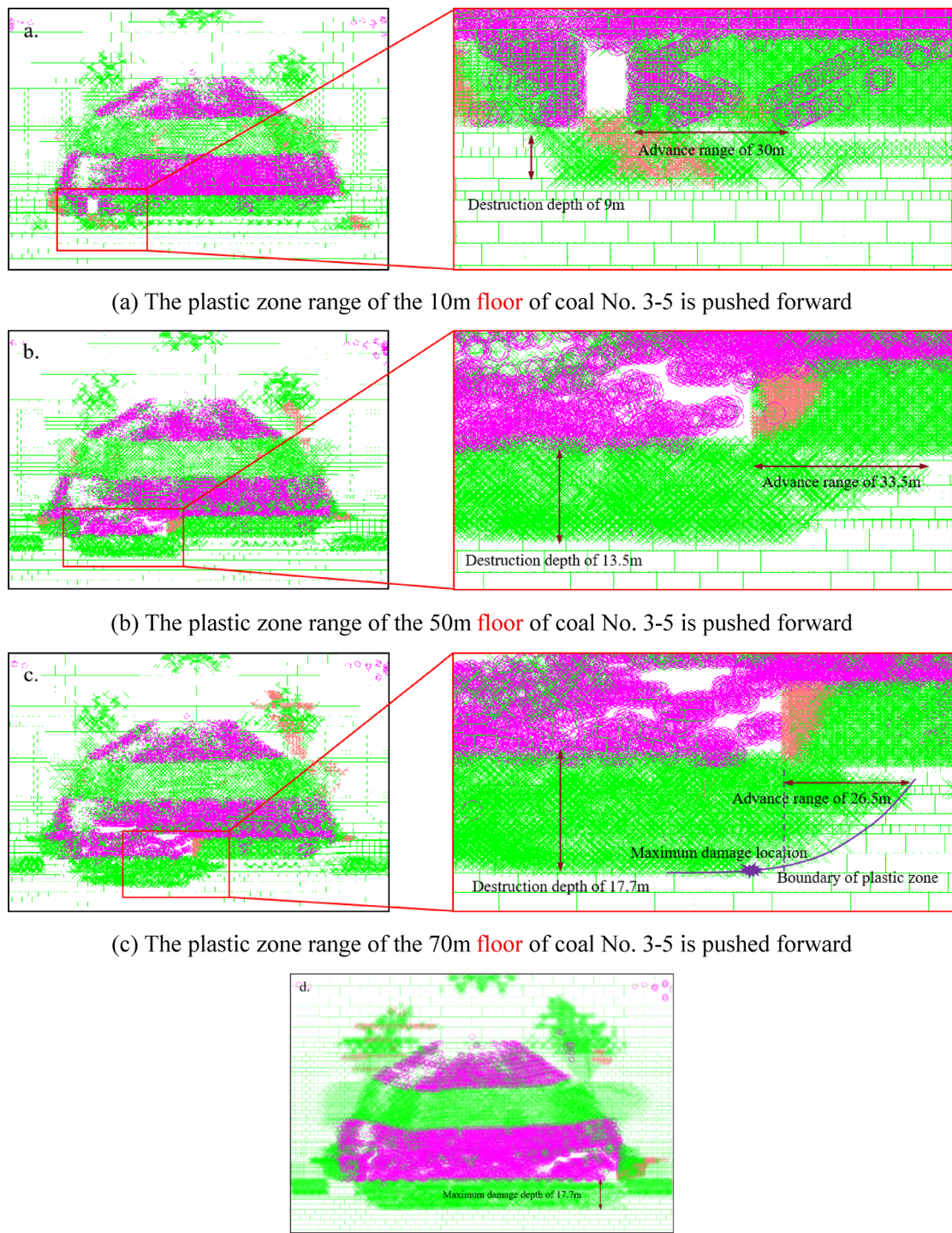
Fig. 6. (**a**) Development characteristics of plastic zone in the mining floor of No. 3–5 coal seams. (**b**) The plastic zone range of the 50 m floor of coal No. 3–5 is pushed forward, (**c**) The plastic zone range of the 70 m floor of coal No. 3–5 is pushed forward, (**d**) The plastic zone range of the 200 m floor of coal No. 3–5 is pushed forward.

pressure, then compressed and stretched, and finally released and restored to the void. The measurement points located in the interlayer transition zone have significant fluctuations, and the maximum damage depth position is clearly characterized by the measurement points. During the self-inspection range of the working face from the beginning to 20 m, the maximum depth position of the floor was compressed to the maximum, and the apparent resistivity was at its maximum. After advancing to 20 m, the maximum depth position of the floor
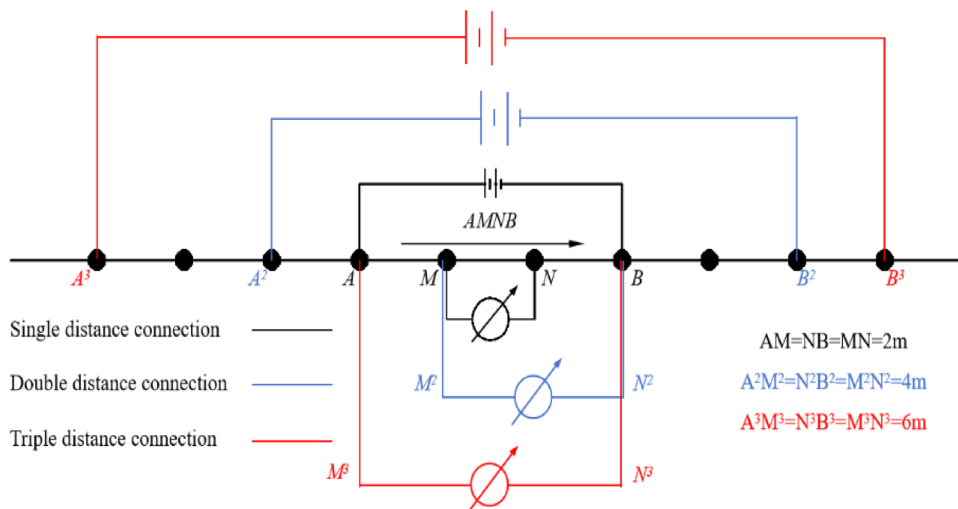
Fig. 7. Principle diagram of symmetrical quadrupole profile method for direct current.
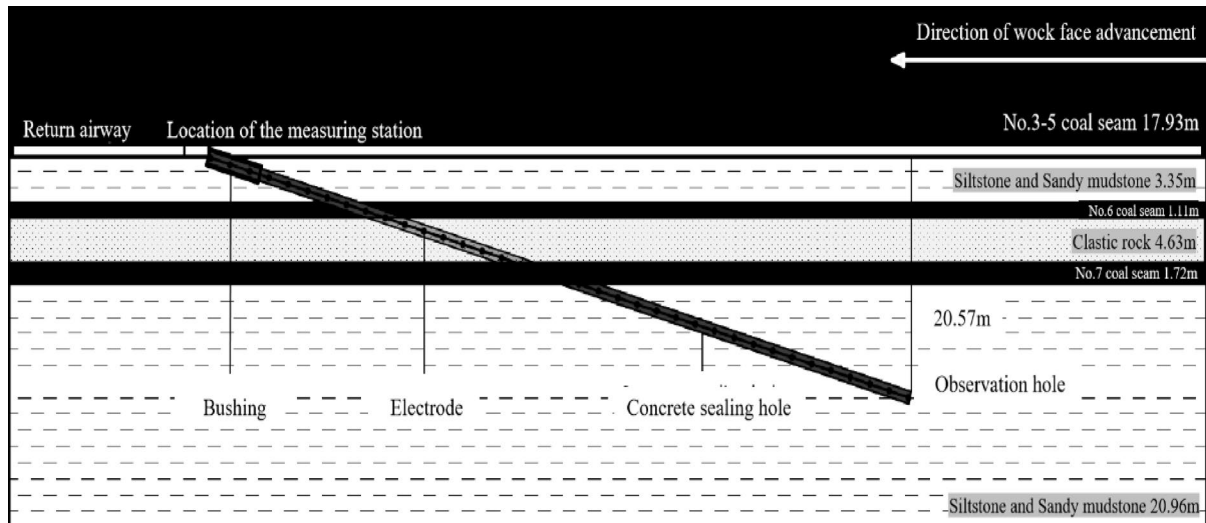

Fig. 8. Relationship between drilling arrangement and bottom rock layer.

was affected by stress recovery, and the apparent resistivity value fell back. After advancing to 45 m, it tended to stabilize and was no longer affected by disturbances. By combining the inclinometer data and using geometric calculations to determine the positional relationship between the working face and the measuring points, that 4–16 m area of the floor has been affected by mining activities, and the maximum damage position is located 16 m behind the working face.

The DC method detection area is a cylindrical rock mass centered on the borehole. By adjusting the distance between the test electrodes (1 to 3 times), the apparent resistivity of the rock mass within a radius of 2–6 m can be measured along the centerline. Figure 13 shows the spatial profile particle relationships along the vertical measurement range of each measuring point along the drilling direction. By connecting the measuring points at all levels according to the test analysis results in this space, curves A and B can be drawn (Fig. 14). Curve A above the drilling hole in the figure conforms to the "saddle shaped" distribution characteristics of the floor failure depth, while curve B is obviously unreasonable. Curve A is the floor failure line, with the maximum position at 28 measuring points. After converting according to geometric relationships, it can be concluded that the maximum depth of damage to the floor of the 30,507 working face is 16.1 m.

Discussion

This study used theoretical analysis, numerical simulation, and on-site measurement methods to investigate the depth and pattern of floor failure in extremely close distance coal seam mining. Based on the on-site measurement results, it can be seen from the error analysis (see Table 3) that the depth and distance calculation results of the elastic-plastic mechanics model are both low, showing errors of 10.74% and 27.31%, respectively.

Number of times	Depth/m	Dip angle/°	Azimuth angle/°
1	5.0	− 19.3	68.2
2	5.5	− 18.8	69.1
3	6.0	− 18.4	69.2
4	6.5	− 18.5	70.3
5	7.0	− 17.7	71.2
6	7.5	− 17.6	70.8
7	8.0	− 17	69.5
8	8.5	− 17	69.4
9	9.0	− 16.2	70
10	9.5	− 15.7	69.7
11	10.0	− 15.9	71.1
12	10.5	− 15	70.6
13	11.0	− 14.4	70.3
14	11.5	− 14.9	70.5
15	12.0	− 13.8	70.5
16	12.5	− 13.2	71
17	13.0	− 13.1	70.6
18	13.5	− 12.5	71.1
19	14.0	− 11.5	70.3
20	14.5	− 10.5	69
21	15.0	− 11.1	70.3
22	15.5	− 10.9	70.6
23	16.0	− 10.7	69.9
24	16.5	− 10.6	69.3
25	17.0	− 9.9	69.6
26	17.5	− 10.2	70.6
27	18.0	− 10	70.6
28	18.5	− 10.9	71.2
29	19.0	− 10.9	71.4
30	19.5	− 11.4	70.4
31	20.0	− 11	69.2
32	20.5	− 11.8	70.5

Table 2. Drilling inclinometer positioning.
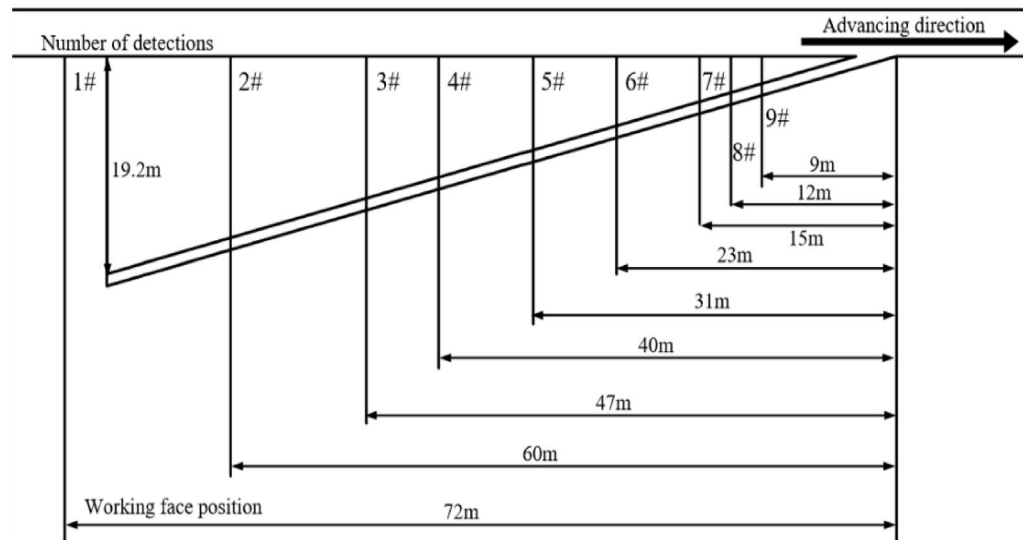
Fig. 9. Relationship between detection process and working face position.
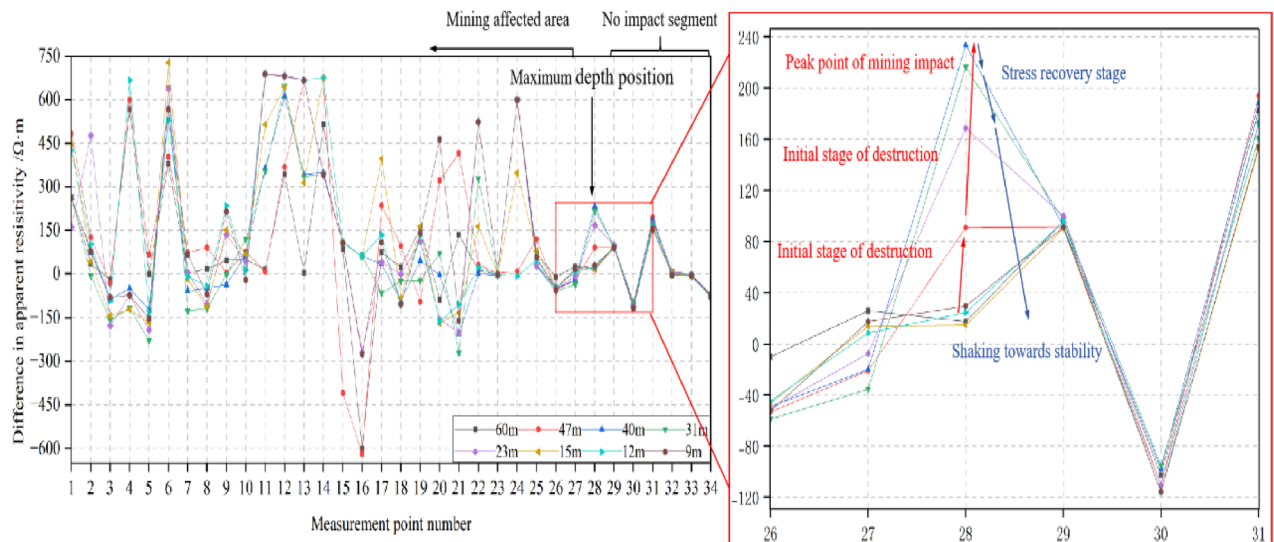
Fig. 10. Differential data of single distance measurement using direct current method.
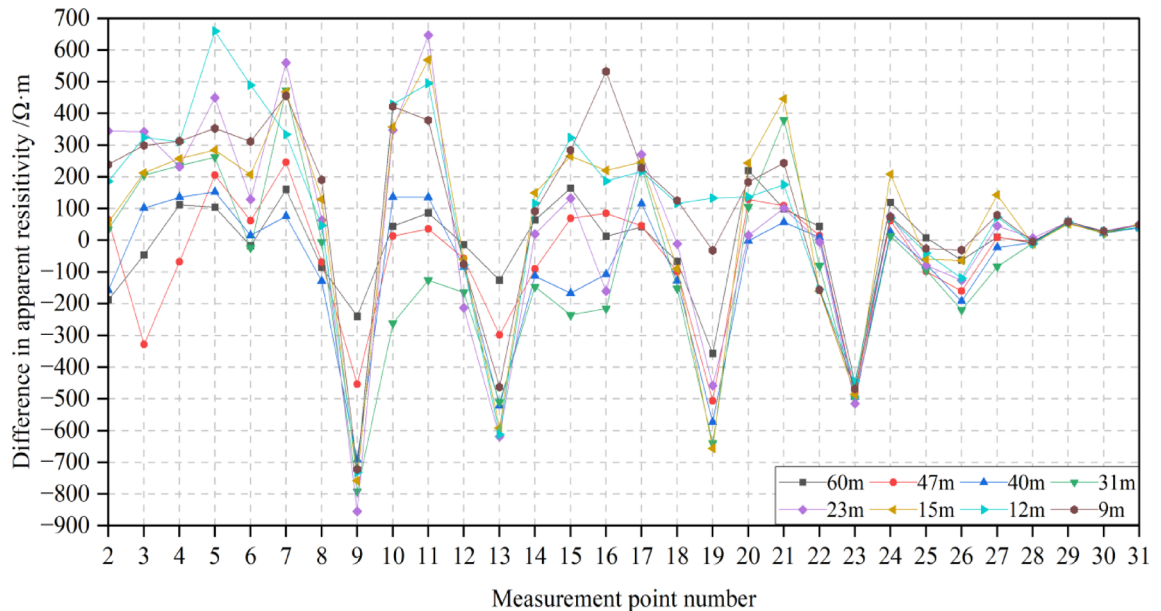
Fig. 11. Differential data for DC method two-fold distance measurements.

This may be due to the limitation of this theory, which regards the rock mass as a homogeneous medium with various isotropic bodies. The damage and pressure relief caused by the mining of the upper coal seam change this property. At the same time, the hard rock mass of the coal seam floor is mainly controlled by the range of stress concentration, and the depth of damage is relatively large. The numerical simulation shows that the depth of damage is relatively large and the distance of damage is relatively small, with errors of 9.94% and 34.375%, respectively. The overall damage process is similar to the measured results, and the shallow area of the leading position is greatly affected by the concentrated stress range. This also confirms the reliability of the measured technology. With the assistance of theoretical calculations and numerical simulations, based on actual measurement results, it can be determined that the maximum depth of damage to the floor of 30,507 in this stage is 16.1 m. In order to ensure safe and efficient production on site and reduce the risk of water inrush from the working face, active detection is the main focus at this stage, supplemented by regional prevention and control, and the control of the construction area is strengthened with appropriate drainage and pressure reduction. We can rely on a low-cost and efficient testing plan in this study to increase the detection of floor damage in high-risk areas.
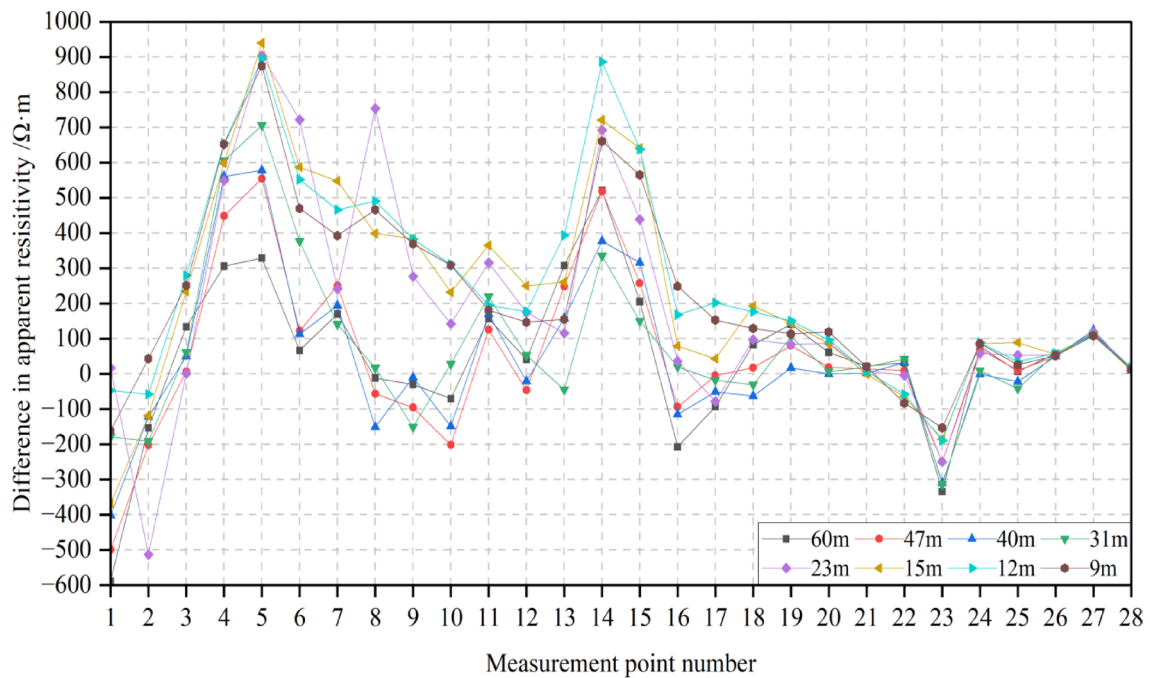
**Fig. 12**. Differential data for DC method triple distance measurements.
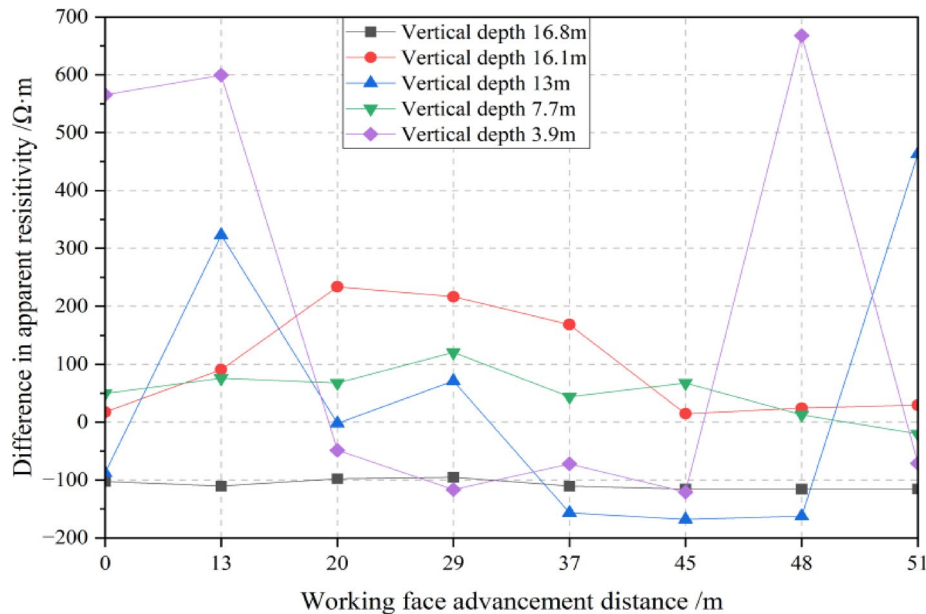
Fig. 13. Changes in apparent resistivity at different depths during the progress of the working face.

Conclusions

(1) The theoretical analysis shows that the floor breaking under the influence of mining is mainly affected by the mechanical properties of the rock strata and the plastic deformation area of the coal wall in front of the working face. It is calculated that the depth of the floor breaking in the 30,507 ultra close working face mining coal seam is 14.37 m, and the breaking position is located in the goaf 11.63 m behind the coal wall.

(2) Numerical simulation studies have shown that the extraction of the upper coal seam at close distance causes significant disturbance to the floor of the lower coal mining face during the initial stage. Shortly after the initial pressure, the floor reaches its maximum damage, with a maximum depth of about 17.7 m, located 10.5 m behind the coal wall.
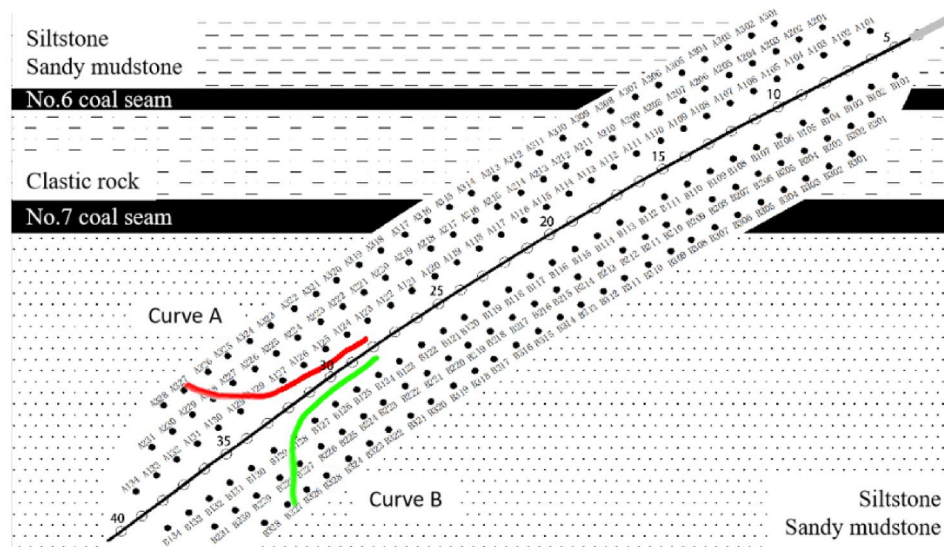
Fig. 14. Test particle distribution and floor failure zone.

Method	Failure depth	Relative error	Lag distance (m)	Relative error
Field measurement	16.10 m		16.00 m	
Theoretical calculation	14.37 m	− 10.74%	11.63 m	− 27.31%
Numerical simulation	17.70 m	+ 9.94%	10.50 m	− 0.34.375%
Average	16.06 m		12.71 m	

Table 3. Comparison of results from different research methods.

(3) Through the symmetrical quadrupole DC profile method, it was found that the failure of the working face floor showed a trend of first compaction, then sliding compression, and finally compaction and stability release. The maximum depth of failure of the measured floor was 16.1 m, lagging behind the working face by 16 m.

(4) The simulation analysis and actual measurement patterns are consistent with theoretical calculations, verifying the reliability and accuracy of single hole DC detection technology in complex environments. The research can provide guidance for the control and detection of coal seam mining floor strata.

Data availability
The datasets generated and/or analyzed during the current study are available from the corresponding author upon reasonable request.

References
1. Pan, W. et al. Top coal drawing law for an extra Thick coal seam under the single round group drawing method. *Sci. Rep.* **14**, 15293 (2024).
2. Pan, W., Nie, X. & Li, X. Effect of premining on hard roof distress behavior: A case study. *Rock. Mech. Rock. Eng.* **52**, 1871–1885 (2019).
3. Jia, J., Zhou, J. Y. & Niu, Q. H. Dynamic evolution characteristics and hazard assessment of microseismic in close repeated mining. *Coal Sci. Technol.* **53** (07), 46–57 (2025).
4. Zhao, Y. X. et al. Stress and fracture evolution patterns in surrounding rock during Close-Proximity coal seam mining with Open-Pit mining. *Chin. J. Coal Sci. Eng.* **47** (01), 259–273. https://doi.org/10.13225/j.cnki.jccs.2021.1526 (2022).
5. Yuan, L. & Zhang, P. S. Development status and prospect of geological guarantee technology for precise coal mining. *J. China Coal Soc.* **44** (8), 2277–2284 (2019).
6. Wu, Q. Progress, problems and prospects of prevention and control technology of mine water and reutilization in China. *J. China Coal Soc.* **39** (5), 795–805 (2014).
7. Sun, C. S. et al. Overburden failure characteristics and fracture evolution rule under repeated mining with multiple key strata control. *Sci. Rep.* **15**, 28029 (2025).
8. Wu, Q., Zhang, Z. L. & Ma, J. F. A new practical methodology of the coal floor water bursting evaluating Ⅰ —The master controlling index system construction. *J. China Coal Soc.* **01**, 42–47 (2007).
9. Ma, D. et al. A state-of-the-art review on rock seepage mechanism of water inrush disaster in coal mines. *Int. J. Coal Sci. Technol.* **9**, 50 (2022).

10. Qi, T. et al. Simulation research and application on response characteristics of detecting water-filled Goaf by transient electromagnetic method. *Int. J. Coal Sci. Technol.* **9**, 17 (2022).
11. Jin, Z. G. & Li, B. Y. Preliminary discussion on mechanism of water inrush from coal floor. *Coal Geol. Explor.* **8** (2), 51–56 (1980).
12. Yang, S. A. Water resistance coefficient and its application. *Coal Geol. Explor.* **14** (3), 41–46 (1986).
13. Liu, Z. C. & Yu, H. Lower three zones theory and mechanism of floor water inrush. *Coal Geol. China*. **3** (2), 38–41 (1991).
14. Wang, L. G. et al. Stress distribution and damage law of mining floor. *J. Min. Saf. Eng.* **30** (3), 317–322 (2013).
15. Wang, Z. Y. & Liu, H. Q. Investigation in floor – water – burst mechanism. *Coal Geol. Explor.* **19** (1), 36–39 (1989).
16. Dong, S. N., Wang, H. & Zhang, W. Z. Judgement criteria with utilization and grouting reconstruction of top ordovician limestone and floor damage depth in North China coalfield. *J. China Coal Soc.* **44** (7), 2216–2226 (2019).
17. Wang, L. G., Bi, S. J. & Song, Y. Numerical simulation of deformation and failure law of floor. *Ground Press. Strata Control*. **21** (4), 35–37 (2004).
18. Wang, Y. D. et al. Contrast of numerical simulation and field measurement on deformation and failure in Thick seam mining floor. *Saf. Coal Mines*. **43** (10), 39–41 (2012).
19. Gong, P. L. et al. Three-dimensional simulation study on law of deformation and breakage of coal floor on mining above aquifer. *Chin. J. Rock Mechan. Eng.* **24** (23), 4396–4402 (2005).
20. Gao, Z. N. & Meng, X. R. Study on deformation and failuring characteristics of seam floor under mining influence. *Min. Saf. Environ. Prot.* **37** (3), 17–20 (2010).
21. Fu, B. J. & Tu, M. Deformation and failure characteristics research on Thick seam mining floor above confined water. *Chin. J. Undergr. Space Eng.* **13** (Sup.1), 107–112 (2017).
22. Xu, Y. C. & Yang, Y. Applicability analysis on statistical formula for failure depth of coal seam floor in deep mine. *Coal Sci. Technol.* **41** (9), 129–132 (2013).
23. Duan, H. F. et al. Field measurement and simulation research on failure depth of fully mechanized thin coal seam floor in Yangcun coal mine. *J. China Coal Soc.* **36** (Sup.1), 13–17 (2011).
24. Zhu, S. Y. et al. Comprehensive measurement of characteristics of deformation and failure of extra-thick coal seam floor induced by fully mechanized top-coal mining. *Chin. J. Geotech. Eng.* **34** (10), 1931–1938 (2012).
25. Wang, H. Z. et al. A comparative study on floor failure law in deep and short distance coal seam mining. *J. Min. Saf. Eng.* **37** (3), 553–561 (2020).
26. Wang, J. C. et al. Application of the electrical profile method in detecting the depth of floor rock destruction in mining face. *Coal Sci. Technol.* **38** (01), 97–100 (2010).
27. Gao, Z. N. & Meng, X. R. The dynamic electrical-detection of coal floor deformation and damage law. *Progress Geophys.* **26** (6), 2204–2209 (2011).
28. Gao, Z. N., Meng, X. R. & Zhao, G. M. DC electrical resistivity CT survey of deformation and damage law of coal floor. *J. Chongqing Univ.* **34** (8), 90–96 (2011).
29. Gao, Z. N., Zheng, Z. W. & Ying, Z. Z. Application of testing technology of electrical method on monitoring overburden failure. *China Coal.* **41** (3), 36–39 (2015).
30. Yue, J. H. et al. Time-lapse change pattern and mechanism of resistivity of coal seam floor mining damage based on inter-hole DC perspective. *J. China Coal Soc.* **49** (1), 601–615 (2024).
31. Daily, W. et al. Electrical resistivity tomography of vadose water movement. *Water Resour. Res.* **28** (5), 1429–1442 (1992).
32. Zhang, F. et al. Application of high-resolution electrical apparatus on confined water mining similar simulation[J]. *Saf. Coal Mines*. **45** (4), 145–148 (2014).
33. Liu, S. C. et al. Research on electrical prediction for evaluating water conducting fracture zones in coal seam floor. *Chin. J. Rock Mechan. Eng.* **28** (2), 348–356 (2009).
34. Zhang, P. S. et al. Comprehensive testing research on floor damage characteristics of mining extra–thick seam in Jungar coalfield. *Coal Geol. Explor.* **49** (1), 263–269 (2021).
35. Wang, C. et al. Application of borehole transient electromagnetic method in detection of floor failure depth in fully mechanized top coal caving face. *Coal Geol. Explor.* **50** (7), 79–84 (2022).

Acknowledgements

Author contributions

WD: conceptualization and methodology, YP: methodology and writing—original draft, SQ and ZN: supervision and conceptualization, DC and MC: investigation and data curation.

Funding

Declarations

Competing interests

The authors declare no competing interests.

Additional information

Correspondence and requests for materials should be addressed to Y.D.

Reprints and permissions information is available at www.nature.com/reprints.

Publisher's note Springer Nature remains neutral with regard to jurisdictional claims in published maps and institutional affiliations.